Acta Oceanol. Sin., 2022, Vol. 41, No. 9, P. 169–181
https://doi.org/10.1007/s13131-022-1993-5
http://www.aosocean.com
E-mail: ocean2@hyxb.org.cn

Arctic summer sea ice phenology including ponding from 1982 to 2017

Xiaoli Chen[1], Chunxia Zhou[1]*, Lei Zheng[2, 3], Mingci Li[1], Yong Liu[1], Tingting Liu[1]

[1] Chinese Antarctic Center of Surveying and Mapping, Wuhan University, Wuhan 430079, China

[2] School of Geospatial Engineering and Science, Sun Yat-sen University, Guangzhou 519082, China

[3] Southern Marine Science and Engineering Guangdong Laboratory (Zhuhai), Zhuhai 519000, China

Received 26 June 2021; accepted 20 November 2021

Abstract

Information on the Arctic sea ice climate indicators is crucial to business strategic planning and climate monitoring. Data on the evolvement of the Arctic sea ice and decadal trends of phenology factors during melt season are necessary for climate prediction under global warming. Previous studies on Arctic sea ice phenology did not involve melt ponds that dramatically lower the ice surface albedo and tremendously affect the process of sea ice surface melt. Temporal means and trends of the Arctic sea ice phenology from 1982 to 2017 were examined based on satellite-derived sea ice concentration and albedo measurements. Moreover, the timing of ice ponding and two periods corresponding to it were newly proposed as key stages in the melt season. Therefore, four timings, i.e., date of snow and ice surface melt onset (MO), date of pond onset (PO), date of sea ice opening (DOO), and date of sea ice retreat (DOR); and three durations, i.e., melt pond formation period (MPFP, i.e., MO–PO), melt pond extension period (MPEP, i.e., PO–DOR), and seasonal loss of ice period (SLIP, i.e., DOO–DOR), were used. PO ranged from late April in the peripheral seas to late June in the central Arctic Ocean in Bootstrap results, whereas the pan-Arctic was observed nearly 4 days later in NASA Team results. Significant negative trends were presented in the MPEP in the Hudson Bay, the Baffin Bay, the Greenland Sea, the Kara and Barents seas in both results, indicating that the Arctic sea ice undergoes a quick transition from ice to open water, thereby extending the melt season year to year. The high correlation coefficient between MO and PO, MPFP illustrated that MO predominates the process of pond formation.

Key words: Arctic sea ice, sea ice phenology, melt timings and durations, melt ponds, remote sensing

Citation: Chen Xiaoli, Zhou Chunxia, Zheng Lei, Li Mingci, Liu Yong, Liu Tingting. 2022. Arctic summer sea ice phenology including ponding from 1982 to 2017. Acta Oceanologica Sinica, 41(9): 169–181, doi: 10.1007/s13131-022-1993-5

1 Introduction

The Arctic sea ice is an indicator of global warming and has undergone remarkable changes during the satellite era. Over this period, its extent (Comiso et al., 2008; Cavalieri and Parkinson, 2012; Peng and Meier, 2018; Onarheim et al., 2018), thickness (Holland et al., 2006; Lei et al., 2012; Lindsay and Schweiger, 2015; Kwok, 2018), volume (Kwok et al., 2009; Kwok and Cunningham, 2015; Kim et al., 2020), and age (Maslanik et al., 2007; Comiso, 2012; Bi et al., 2018) have decreased drastically. Phenology factors that reflect changes in the Arctic sea ice are crucial to business strategic planning and climate monitoring (Peng et al., 2018). These factors are useful for sea ice simulation to improve the seasonal sea ice forecasts with more details on sea ice evolution. Information on how does the Arctic sea ice evolve and what are decadal trends in ice phenology factors during melt season is necessary under global warming.

Date of snow and ice surface melt onset (MO) marks the day that snow and ice surface start melting at the beginning of the melt season. On this day, snow and ice albedo starts to decrease slightly. Decreased surface albedo initiates the positive sea ice-albedo feedback mechanism (Curry et al., 1995), thereby controlling the total energy input into the ice-ocean system (Bliss et al., 2017; Perovich et al., 2007). Moreover, information on surface melt conditions is needed to monitor sea ice extent trends (Matthews et al., 2020). Evaluation of pan-Arctic and regional MO has been conducted. Markus et al. (2009) demonstrated a negative trend in MO since 1979 except for the Sea of Okhotsk over the Arctic by utilizing passive microwave (PMW) data. Kouki et al. (2019) compared MOs retrieved from optical and microwave satellite data in the Arctic between 1982 and 2015, and the results suggested an overall areal-mean 10 days earlier in optical-based MO and a significant negative trend in MO. In addition, MO derived from surface air temperature with a –1.0°C threshold were about 11 days later than those from PMW data, whereas both results indicated a coherent decreasing trend in the Arctic since 1979; the most negative trends of –9.5 d/decade were observed in the East Siberian Sea (Bliss and Anderson, 2018). Nevertheless, according to synthetic aperture radar data, no significant trend in MO was detected in the northern Canadian Arctic Archipelago from 1997 to 2017 (Mahmud et al., 2016).

Shortly after the onset of sea ice surface melt, meltwater begins to collect in surface depressions and forms visible pools on

Foundation item: The National Key Research and Development Program of China under contract No. 2018YFC1406102; the Funds for the Distinguished Young Scientists of Hubei Province (China) under contract No. 2019CFA057; the National Natural Science Foundation of China under contract Nos 41941010 and 41776200.
*Corresponding author, E-mail: zhoucx@whu.edu.cn

low permeable ice; these pools are referred to as melt ponds (Polashenski et al., 2012). Pond-covered ice has a lower albedo of between 0.2 and 0.4 compared with snow-covered ice of about 0.8 and bare ice of between 0.5 and 0.6; thus, pond-covered ice undergoes further surface melting and stores and transmits more solar energy to the ocean (Untersteiner, 1961; Perovich et al., 2002). Melt ponds contribute to one of the largest uncertainties on the Arctic sea ice prediction due to their effects on the surface heat budget (Flocco et al., 2012; Holland et al., 2012; Hunke et al., 2013). Typically, multi-year ice is characterized by a lower melt pond fraction (MPF) compared with first-year ice due to the topographic limit (Grenfell and Perovich, 2004; Landy et al., 2015; Li et al., 2017b). The most widely applied approach to detect MPF is optical remote sensing (Markus et al., 2003; Tschudi et al., 2008; Rösel et al., 2012; Istomina et al., 2015b; Webster et al., 2015; Li et al., 2020). Nonetheless, with the restriction of cloud cover in optical satellite imagery, MPF generated from microwave data has been conducted as well (Scharien et al., 2014; Fors et al., 2017; Li et al., 2017a). A vast majority of these studies focused on optical properties (Light et al., 2015; Lu et al., 2018a; Nicolaus and Katlein, 2013), morphological observations (Huang et al., 2016; Istomina et al., 2015a; Lu et al., 2018b), and simulation of melting process (Flocco et al., 2015; Ma et al., 2019; Scott and Feltham, 2010). However, our understanding of the ponding time over the Arctic is still sparse (Zheng et al., 2017).

With the development of surface melting, sea ice concentration (SIC, i.e., the fractional cell coverage of sea ice within a grid) decreases. Steele et al. (2015) put forward the date of opening (DOO, i.e., SIC drops below 80%) combined with the date of retreat (DOR, i.e., SIC drops below 15%); they outperform sea ice extent and area in illustrating the evolution of Arctic sea ice. DOO marks the start of the seasonal ice loss phase, whereas DOR captures the end of sea ice loss (Steele and Dickinson, 2016). The trends in DOR over the Arctic were investigated, and the results showed the trend of earlier ice retreat (Stammerjohn et al., 2012). Maximum sea surface temperature plays an important role in triggering ice retreat (Steele and Dickinson, 2016).

There are many studies on phenology factors separately, yet few studies integrated them to track sea ice evolvement. Several researchers examined the temporal means and trends of a suite of phenology factors in the Arctic, including MO, DOO, and DOR (Peng et al., 2018; Bliss et al., 2019). They concluded that a large regional variability was present in the means and trends of the three aforementioned factors, which are becoming earlier over the Arctic. However, previous studies of the Arctic sea ice phenology did not involve melt ponds, which affect the process of sea ice surface melt tremendously (Polashenski et al., 2012).

For the first time, we presented an analysis of temporal means and trends of a series of phenology factors, including PO and its corresponding periods of the Arctic melting sea ice from 1982 to 2017. Therefore, four timings, i.e., MO, PO, DOO, and DOR, and three durations, i.e., melt pond formation period (MPFP, i.e., MO–PO), melt pond extension period (MPEP, i.e., PO–DOR), and seasonal loss of ice period (SLIP, i.e., DOO–DOR), were used. In addition, differences in factors derived from Bootstrap and NASA Team SIC (henceforth known as BT SIC and NT SIC, respectively) were compared.

The paper is organized as follows. The study area and datasets are outlined in Section 2. Section 3 describes the methodology to evaluate PO and the principles of obtaining regional statistics. In Section 4, the temporal means and variability of these timings and periods are exhibited, as well as the statistics results are discussed in terms of results, followed by the conclusions in Section 5.

2 Study area and datasets

2.1 *Study area*

Following Cavalieri and Parkinson (2012), the Arctic was divided into eight different sectors (Fig. 1), namely, the Sea of Okhotsk, the Bering Sea, the Arctic Ocean, the Canadian Arctic Archipelago, the Hudson Bay, the Baffin Bay, the Greenland Sea, and the Kara and Barents seas. Open water out of the Arctic Circle and the North Pole hole within the Arctic Ocean is depicted in white and are not discussed in this study. Although the Sea of Okhotsk, the Bering Sea, and the Baffin Bay are outside the Arctic Circle, they were important because of the extensive coverage of sea ice and were examined in this study.

2.2 *Datasets outline*

MO were obtained directly from the data set containing snowmelt onset dates over the Arctic sea ice archived at the National Snow and Ice Data Centre (NSIDC) (Anderson et al., 2019). The dates are estimated using the Advanced Horizontal Range Algorithm (AHRA) based on the daily brightness temperatures from the Scanning Multichannel Microwave Radiometer, Special Sensor Microwave/Imager, and Special Sensor Microwave Imager/Sounder (Anderson, 1997; Bliss and Anderson, 2018). The datasets are mapped to a 25 km NSIDC polar stereographic grid in flat binary with 448 rows and 304 columns using Hughes' 1980 ellipsoid.

The timings of PO were determined by using sea ice albedo product from the extended Advanced Very High Resolution Radiometer (AVHRR) Polar Pathfinder (APP-X). The product was archived at the NOAA/NSIDC climate data record (CDR) (Key et al., 2016). The dataset was mapped to a 25 km EASE-Grid in flat binary with 361 rows and 361 columns. Considering that over 50% of data on the sea ice albedo product was missed in winter and the time ice started ponding, only albedo from the Day of Year 90 (early April) to 260 (middle of September) were used to calculate the PO.

The DOO and DOR were identified from the time series of daily passive microwave SIC products by applying two well-es-

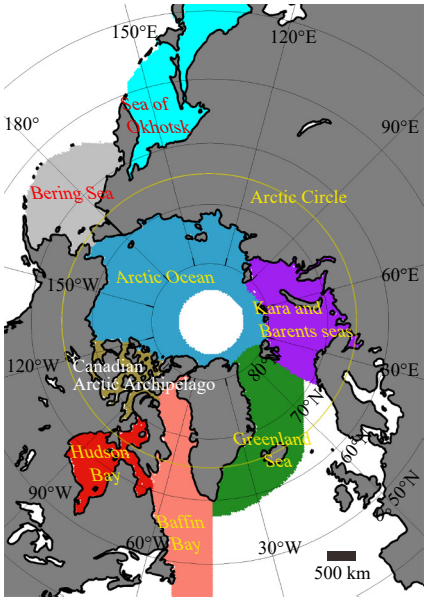

Fig. 1. Map of the Arctic and eight sectors. The land masses shown in dark grey are omitted from the regional analysis.

tablished algorithms, namely, NASA Team (Cavalieri et al., 1984) and Bootstrap Algorithm (Comiso, 1995). These SIC products were generated from brightness temperature data, which were the same source data utilized for MO; these data were mapped on the NSIDC polar stereographic grid with nominal 25 km × 25 km grid cells. The acronyms and definitions for these factors are shown in Table A1.

3 Methods

3.1 *PO detection*

The sensitivity of sea ice albedo to surface meltwater was employed to detect ponding date. Before the onset of surface melt, both first-year ice and multi-year ice are covered by snow. The snow-covered first-year ice and multi-year ice are characterized by commonly high and stable albedo, and their albedos are nearly the same (Perovich and Polashenski, 2012). A slight decrease occurs when snow and ice surface start melting, but a dramatic decrease takes place when ponding begins. Considering this characteristic, identifying PO was possible by utilizing an empirical linear function associating sea ice albedo and pond fraction (Rösel and Kaleschke, 2012), as follows:

$$A_{\mathrm{TR}} = A_0 - A_1 \times \mathrm{MPF}, \tag{1}$$

where A_0 and A_1 are coefficients; MPF is the melt pond fraction, defined as the ratio between the melt ponds area and sea ice area in a grid cell. The coefficients are set following Zheng et al. (2017), i.e., A_0 = 0.62 and A_1 = 0.45. Thus, we obtained different sea ice albedo thresholds A_{TR} according to the varied MPFs. Once sea ice albedo is reduced to A_{TR} as the melt season progressed, PO is detected. The sea ice albedo (α_{i}) can be estimated by using composite albedo (α, i.e., satellite-derived albedo) and sea ice concentration (Lei et al., 2016), as follows:

$$\alpha = C_{\mathrm{w}}\alpha_{\mathrm{w}} + C_{\mathrm{i}}\alpha_{\mathrm{i}}, \tag{2}$$

where C_{w} and C_{i} are the area fractions of open water and sea ice, and α_{w} and α_{i} are their albedos, respectively. The albedo of open water can be set to 0.07 as being put forward by Pegau and Paulson (2001). Sensitivity test results suggested that a slight shift in the MPF threshold between 0.01 and 0.30 did not change the result much. Therefore, we opined that ice surface started ponding when the MPF reached 10% (A_{TR} = 0.575) as used by Zheng et al. (2017), which allowed most of the derived PO to occur between MO and DOR.

3.2 *Regional statistics*

Owing to the dramatic decrease in albedo that results from melt ponds, the radiative balance in the Arctic changes. Moreover, the flux of absorbed solar energy is increasing and the surface melting progress is speeding up due to the positive feedback mechanism. However, meltwater can collect and thereby form melt ponds only if the ice surface has depressions and low permeability. This phenomenon creates a quandary for generating a time series of sector-wide mean arguments with respect to the area over which an average can be obtained.

Two strategies were used in regional analyses, as follows: (1) the average was obtained in each year over the area where an argument is valid, and this approach was referred to as Method I; (2) the average was obtained in each year only over the area where the sea ice experiences MO, PO, and DOR chronologically, and this approach was referred to as Method II. Results obtained using Method I disclosed the interannual variability of each parameter in regional means, whereas those obtained using Method II exhibited a full evolution of ice surface melting progress on ponding ice. In Method II, we masked all timings and durations to locations that have a valid PO. Parameters determined from BT SIC and NT SIC are named with prefixes "b" and "n", respectively. For example, bPO and nPO represented the PO determined from BT SIC and NT SIC, respectively.

An analysis of regional trends for every factor was conducted using both strategies mentioned above. Both regional trends in all factors only counted the locations where a parameter was present for at least 80% of the years over the entire record, i.e., more than 29 years. The flow chart of data processing for this work is presented in Fig. 2.

4 Results and discussion

4.1 *Spatial distribution of timings*

The mean MO for the Arctic over 1982–2017 (Fig. 3a) shows high latitudinal dependence on earlier surface melting starting from March and April in the southernmost latitudes and along the marginal seas, i.e., the Sea of Okhotsk, the Bering Sea, the south of Baffin Bay, the Greenland Sea, the Barents Sea, and the periphery of Hudson Bay. As the summer progressed, the MO spread northward. The latest surface melting region was in the central Arctic Ocean and the northern Canadian Arctic Archipelago, where ice surface started melting during June–July. The MO began in other sectors between April and June, such as the Kara Sea, the outer of the Arctic Ocean, the majority of the Hudson Bay, the northern Baffin Bay, and the coast of the northern Greenland Sea.

The linear trends of the Arctic MO were examined. Decadal trends in MO from 1982 to 2017 were computed and shown in Fig. 3b. The Arctic presented striking negative trends in general. The largest trends were over –6 d/decade in the Kara and Bar-

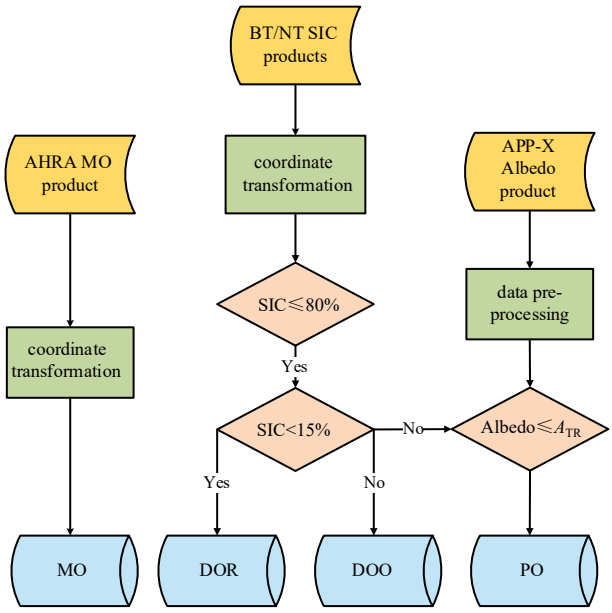

Fig. 2. Flow chart of data processing. BT/NT: Bootstrap and NASA Team; SIC: sea ice concentration; AHRA: Advanced Horizontal Range Algorithm; MO: melt onset; DOR: date of retreat; DOO: date of opening; PO: pond onset.

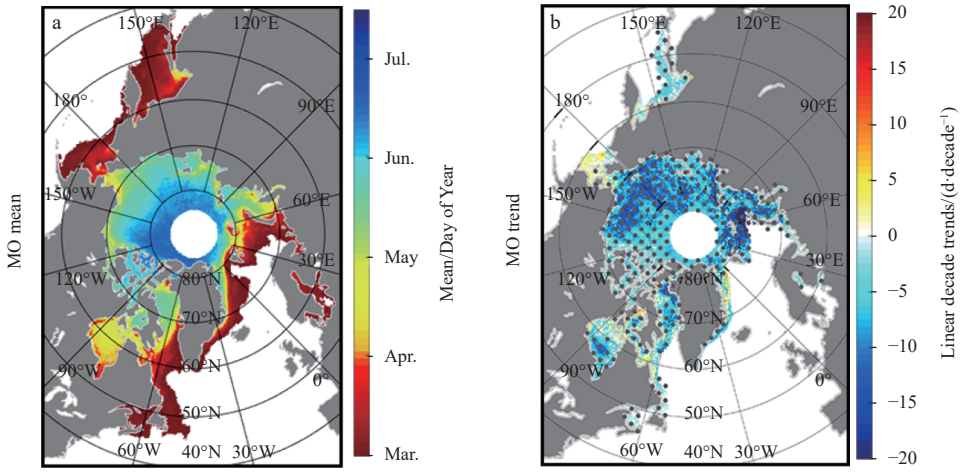

Fig. 3. Mean (a) and linear decadal trends (b) of melt onset (MO) for the period of 1982–2017. Trends are calculated only in locations where MO occurs in more than 80% of the years over the entire record. Black points indicate that the trends are significant at the 95% confidence level.

ents seas and the Arctic Ocean (Table 1), which indicated a shift toward an earlier MO over the last 36 years. The largest downward trend in the Barents and Kara seas may be partly associated with the decreased cooling efficiency in the Barents Sea over the past decades (Skagseth et al., 2020; Shu et al., 2021). The intensified decrease in sea ice that occurred in Chukchi and Beaufort seas from 2000 to 2012 was in accordance with the second-largest significant downward trend in the Arctic Ocean (Frey et al., 2015). Notably, a slightly positive trend, which was statistically non-significant in MO with 1.5 d/decade, was observed in the Bering Sea. The accelerated increase in sea ice cover that resulted from lower temperature and cold northerly wind in 2006–2012 may in part explain the later MO in the Bering Sea (Frey et al., 2015).

The mean PO and its trends derived from the BT and NT SIC for 1982–2017 are presented in Fig. 4. In addition, the differences

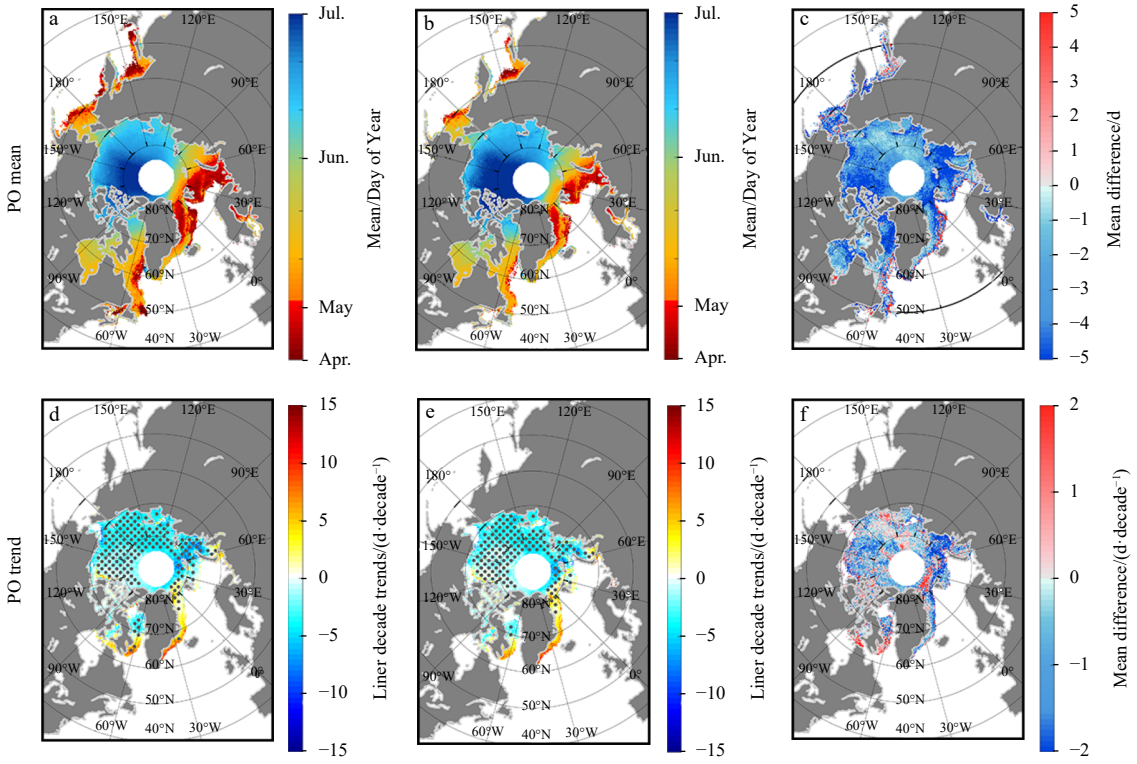

Fig. 4. Mean and linear decadal trends of pond onset (PO) for the period of 1982–2017 were derived by Bootstrap Team sea ice concentration (BT SIC), i.e., bPO mean (a) and bPO trend (d), and NASA Team sea ice concentration (NT SIC), i.e., nPO mean (b) and nPO trend (e). The differences (BT result minus NT result) between the two estimations (c, f) are shown. Trends are calculated only in locations where PO occurs in more than 80% of the years over the entire record. Black points indicate that the pixels are significant at the 95% confidence level.

determined by these two SIC products are shown in Figs 4c and f. As expected, both average PO showed an evident latitudinal dependence, which was consistent with the process of the MO. The difference between mean bPO and nPO ranged from –5.1 d in the Bering Sea to –2.5 d in the Hudson Bay, and the overall difference was –4 d. The melt ponds began to form earliest in the peripheral seas in late April in the BT and NT results, except for the southeastern Baffin Bay and the southern Greenland Sea, in which ice started ponding from early to middle May. As shown in Figs 4a and b, meltwater started to collect and subsequently resulted in PO in the Hudson Bay, inner Baffin Bay, and the Kara Sea from May to June. The Arctic Ocean, the Canadian Arctic Archipelago, and the north of Baffin Bay started ponding during June. Corresponding with the latest MO, the Arctic Ocean ponding occurred latest in late June.

Decadal trends in the date of bPO and nPO were quite similar with the largest discrimination less than 2 d/decade (Fig. 4f), and exhibited a weak, increasing trend on the whole (Table 1). Both PO presented negative trends, except for the Sea of Okhotsk, the Bering Sea, the Hudson Bay, the Baffin Bay, and the Greenland Sea (Figs 4d, e; Table 1). Graphically, the greatest downward trends were presented in most Barents-Kara sea in both PO trends, whereas the regional-mean even exhibited a later ponding trend in nPO due to the upward trend along the coast of Barents-Kara sea, which may have resulted from the increase in the amount of ice that drifted from the north and got stuck along the coastal area from 1981 to 2010 (Kumar et al., 2021). Significant positive trends in the Bering Sea and the Hudson Bay were observed both in bPO and nPO. The largest upward trend occurred in the Sea of Okhotsk because the counted locations were few. The most significant downward trends were found in the Arctic Ocean with –2.6 d/decade and –2.3 d/decade in bPO and nPO, respectively (Figs 4d, e; Table 1). It may be partly explained by the notable reductions in sea ice cover observed in the Chukchi and Beaufort seas of the Pacific Arctic Region (Steele et al., 2008; Stroeve et al., 2012; Frey et al., 2015).

As exhibited in Fig. 5, the DOO (Figs 5a, b) and DOR (Figs 5g, h) extracted from BT and NT SIC started in the peripheral seas and spread northward as the melt season progressed in general, except the Hudson Bay. On the whole, DOO and DOR determined by BT SIC occurred later than NT SIC (Fig. 5c). The exceptional areas were a few locations in the Sea of Okhotsk, the Bering Sea, and the southern Baffin Bay. The most remarkable areal-mean differences between bDOO and nDOO, which were over 30 days, were observed in the Hudson Bay and the Arctic Ocean. Both DOOs began in April along marginal seas, whereas the latest DOO from NT SIC occurred in early July within the Arctic Ocean. The nDOO was 16 days earlier in contrast to bDOO, which was attributed to the larger disagreement between BT SIC and NT SIC in the seasonal ice zone in spring with much lower NT SIC, whereas the most similar SIC in June and July contributed to less dissimilarity in DOR (Comiso et al., 1997). Similarly, bDOR occurred during March–October in contrast to nDOR in April–September with respect to the corresponding DOO. A negative difference was observed in a part of the central Arctic Ocean, thereby indicating that bDOR occurred earlier than nDOR (Fig. 5i). This phenomenon resulted from the larger NT SIC than BT SIC in that location.

The vast majority of the Arctic was predominated by negative trends in DOO and DOR obtained from both SIC products, indicating a pronounced shift toward earlier sea ice retreat (Figs 5d, e, j, k). The total areal-mean trend was approximately 4 d/decade earlier in both DOO trends and over 5 d/decade advanced in both DOR trends (Table 1). Graphically, all seas exhibited downward trends in both DOO trends, except for the southeast part of the Hudson Bay in bDOO. A pronounced difference was found between the trends of the two DOO; fewer locations had valid trends in bDOO due to less ice cover opening over the 36-year study period in BT SIC (Figs 5d, e). Considering the inflow of warm water from the North Atlantic Ocean and the interaction between ocean and atmosphere (Kumar et al., 2021), the greatest significant negative trends were observed in the Kara and Barents seas in both DOOs with more than 10 d/decade, as well as in both DORs with about 8 d/decade (Table 1). In general, almost all regions showed greater negative trends in bDOR than nDOR, as shown in Fig. 5l. Similar to the Beaufort Sea, the spatial variations in DOO and DOR derived from two SIC across the Arctic have been shrinking over the past 36 years, as thicker ice trending toward earlier dates were greater in amount than thinner ice (Steele et al., 2015); thus, DOO and DOR are becoming more synchronous (Wu and Wang, 2019; Wang et al., 2020).

Table 1. Regional decadal trends (d/decade) in phenology factors are presented. All locations with a valid parameter were included. Except for MO, the first and second rows for each factor represent the results derived from Bootstrap and NASA Team, respectively

Indicators	All	Sea of Okhotsk	Bering Sea	Hudson Bay	Baffin Bay	Greenland Sea	Kara & Barents seas	Arctic Ocean	Canadian Arctic
MO (BT/NT)	–0.6**	–0.3	0.2	–2.4	–1.3*	–0.5	–5.0**	–6.4**	–2.6**
PO (BT)	0.7	4.6	3.9*	2.6*	1.5	2.6**	–0.5	–2.6**	–0.7
PO (NT)	1.0	4.2	3.6*	1.9	1.5	3.0**	0.6	–2.3**	–0.9
DOO (BT)	–5.8**	–5.6	–0.7	–2.2	–6.9**	–2.2*	–12.1**	–2.5*	–3.2**
DOO (NT)	–4.5**	–4.3*	3.6	–2.4	–5.4**	–1.3	–10.3**	–3.7**	–2.2*
DOR (BT)	–4.1**	–2.0	–2.0	–6.3**	–5.3**	–3.1*	–8.6**	–3.2**	–5.2**
DOR (NT)	–2.7**	–1.1	–0.9	–5.1**	–4.5**	–1.2	–7.9**	–1.5	–2.3*
MPFP (BT)	–0.2	–2.2	–2.7	0.2	–0.9	1.7	1.4	1.7**	–0.1
MPFP (NT)	0	–2.7	–3.0*	–0.5	–0.9	2.4*	2.3**	1.9**	–0.2
MPEP (BT)	–0.2	–4.8**	–1.7	–4.6**	–4.1**	–4.8**	–5.2**	–0.8	–2.8*
MPEP (NT)	0.2	0.3	0.5	–3.5**	–3.5*	–4.3**	–5.8**	0.3	0.2
SLIP (BT)	–3.3**	–2.1*	2.0	–3.0**	–3.0**	–3.9	–2.5**	–2.6**	–3.8**
SLIP (NT)	–2.9**	–2.3	–4.4	–1.7	–3.6	–6.5	–3.0	1.5	–1.1

Note: Significant levels of trends are noted as 95% (*) and 99% (**). MO: melt onset; PO: pond onset; DOO: date of sea ice opening; DOR: date of sea ice retreat; MPFP: melt pond formation period; MPEP: melt pond extension period; SLIP: seasonal loss of ice period; BT: Bootstrap Team; NT: NASA Team.

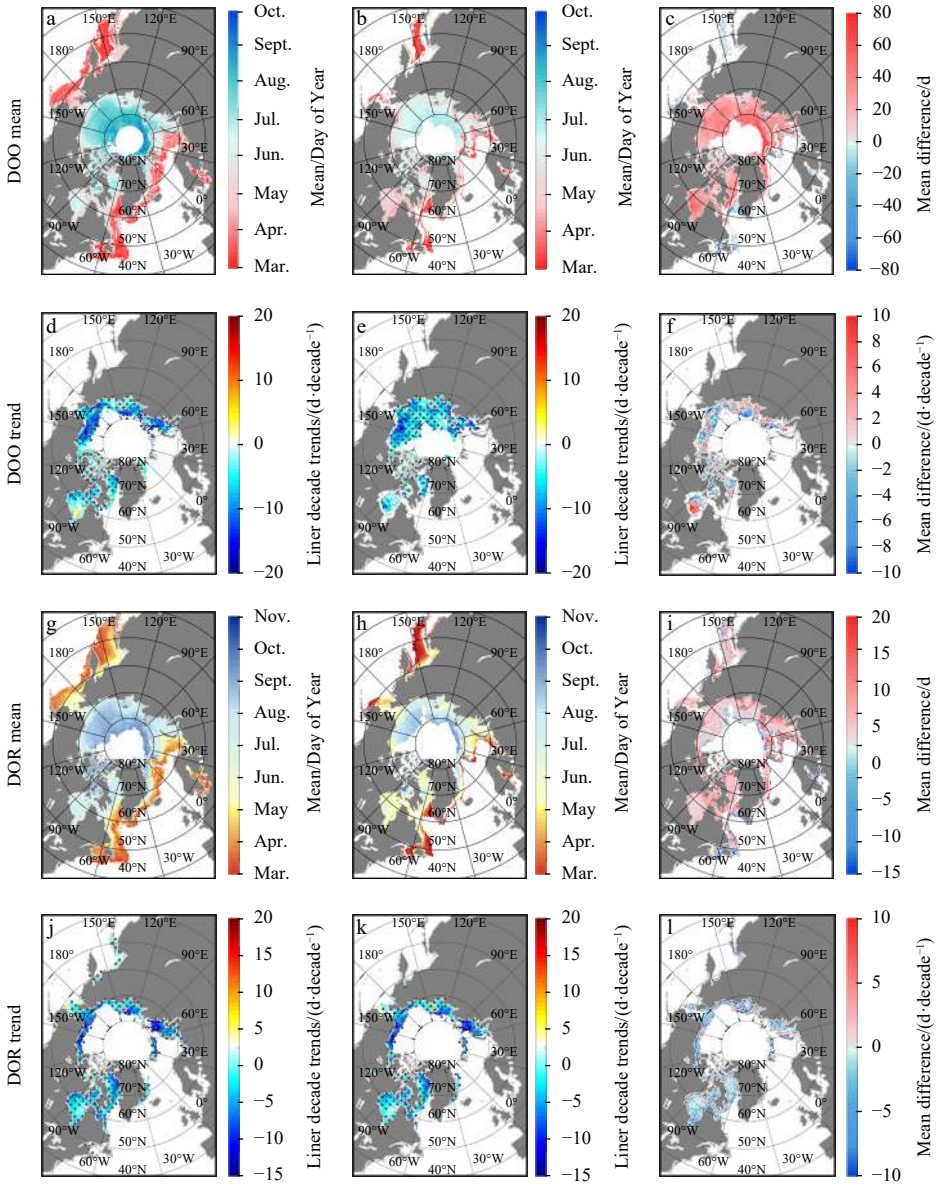

Fig. 5. Mean and linear decadal trends in DOO and DOR for the period of 1982–2017 derived from BT SIC, i.e., bDOO mean (a), bDOO trend (d), bDOR mean (g), bDOR trend (j), and NT SIC, i.e., nDOO mean (b), nDOO trend (e), nDOR mean (h), nDOR trend (k). The differences (BT result minus NT result) of the four estimations (c, f, i, and l) are also shown. Trends are calculated only in locations where DOO or DOR occurs in more than 80% of the years over the entire record. Black points indicate that the trends are significant at the 95% confidence level.

4.2 *Spatial distribution of durations*

The mean date and linear decadal trends of melt pond formation period (MPFP) and MPEP derived from the BT and NT SIC for 1982–2017 and their differences are presented in Fig. 6. The area-averaged MPFP obtained from Bootstrap results varied between 24 d in the Canadian Arctic Archipelago and 56 d in the Bering Sea. The bMPFP was generally shorter than nMPFP and their differences ranged from –5.4 d to –2 d in the Bering Sea and the Hudson Bay, respectively. (Figs 6a–c; Table A2). Graphically, bMPFP lasted around 20 d in the Sea of Okhotsk, the Arctic Ocean, the Canadian Arctic Archipelago, the northern Baffin Bay, the western Greenland Sea, and the Kara Sea (Fig. 6a). The bMPFP appeared longer in the Hudson Bay, the central Baffin Bay, the eastern Greenland Sea, and the Barents Sea with lower latitudes, varying from 40 d to 60 d. The longest bMPFP occurred in the southern Baffin Bay and along the southernmost edge of marginal seas, i.e., the Sea of Okhotsk, the Bering Sea, and the Greenland Sea, where the bMPFP exceeded 60 d. The regional mean in bMPEP ranged from 18.9 d in the Bering Sea to 87.5 d in the Greenland Sea, and the overall areal-mean was 4.8 d longer than that from nMPEP (Figs 6g–i; Table A2). Interestingly, MPEP exhibited the exact inverse pattern to MPFP in BT and NT results and the differences between the two results are mostly in 10 d. The longest MPEP exceeded 80 d in the highest latitudes, i.e., the east of the central Arctic Ocean and northern Greenland Ocean, and in the Canadian Arctic Archipelago and the northern Hudson Bay, where sea ice had a complex topography. Shorter MPEP was observed in the outer and western Arctic Ocean and the ma-

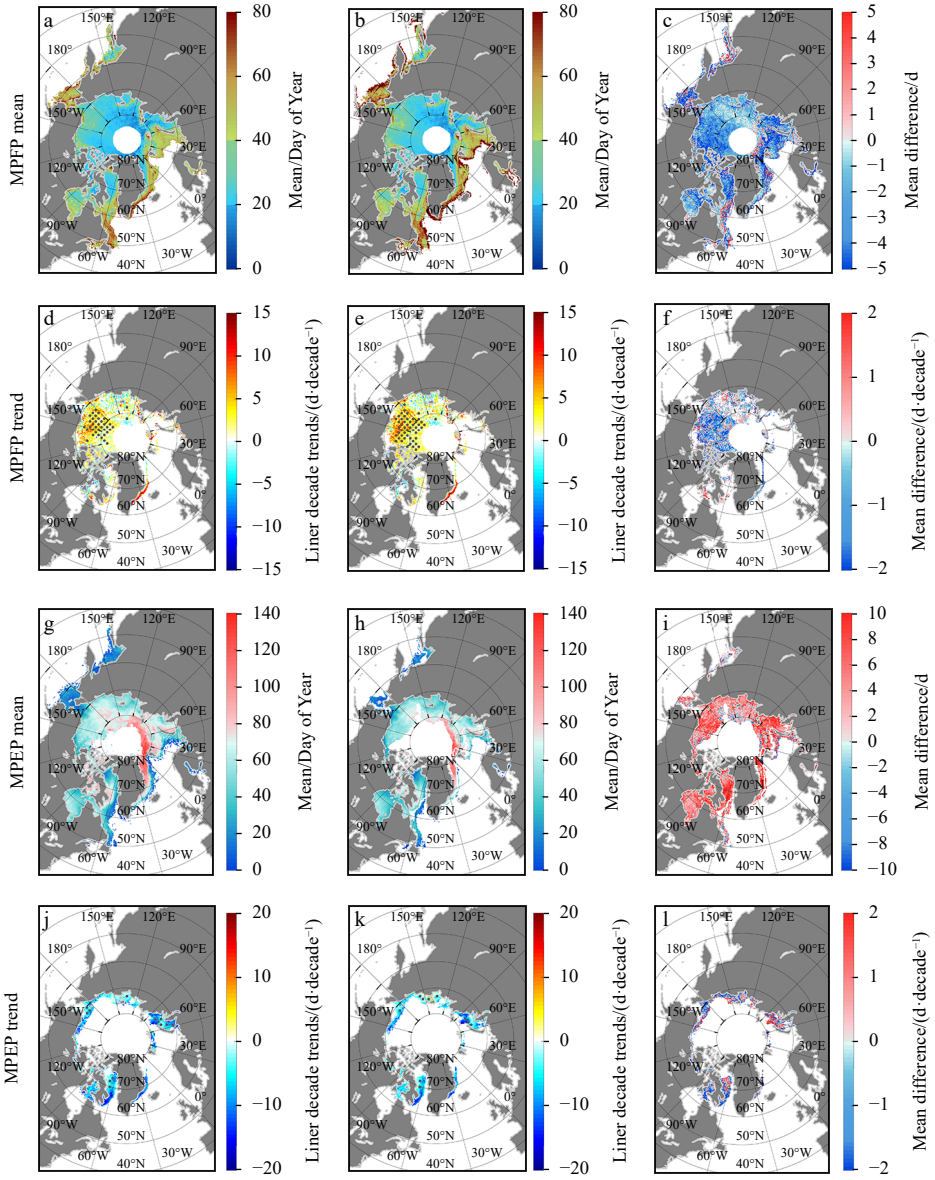

Fig. 6. Mean and linear decadal trends of melt pond formation period (MPFP) and melt pond extension period (MPEP) for 1982–2017 derived from Bootstrap Team sea ice concentration (BT SIC), i.e., bDOO mean (a), bDOO trend (d), bDOR mean (g), and bDOR trend (j), and NASA Team sea ice concentration (NT SIC), i.e., nDOO mean (b), nDOO trend (e), nDOR mean (h), and nDOR trend (k). The differences (BT result minus NT result) of the four estimations (c, f, i, l) are also shown. Trends are calculated only in locations where MPFP or MPEP occurs in more than 80% of the years over the entire record. Black points indicate that the trends are significant at the 95% confidence level.

jority of Hudson Bay in BT and NT results. The bMPEP was shortest along the peripheral sea ice edge, where bMPEP was less than 20 d.

Graphically, the trends of MPFP derived from BT and NT results were in good agreement with the greatest discrimination of no more than 2 d/decade, except in the Hudson Bay in which suggested opposite trends (Figs 6d–f; Table 1). In general, although statistically non-significant inverse trends of MPFP over the Arctic were observed in BT and NT results, the trends were near zero (Table 1). Nevertheless, the Arctic Ocean and the Kara and Barents seas exhibited statistically significant positive trends in MPFP in both results. The most increasing trend in MPFP was observed in the Greenland Sea, whereas the trend was significant in nMPFP only. Similar to MPFPs, MPEPs derived from BT and NT results were comparable, and their disparities over the Arctic were within 2 d/decade (Fig. 6l). Therefore, the MPFP and MPEP we presented above are convictive. Significant negative trends were presented in the Hudson Bay, the Baffin Bay, the Greenland Sea, and Kara and Barents seas in both results. In other words, less time was needed for ice to melt out since the pond onset, i.e., the sea ice transmitted from full ice cover to open water more quickly, thereby extending melt season (Zheng et al., 2021); more heat was absorbed by the ocean, thereby contributing to delaying the winter freezing (Stroeve et al., 2012).

In general, the SLIP detected from BT SIC was approximately 14 d shorter than NT SIC except for the edge of marginal seas,

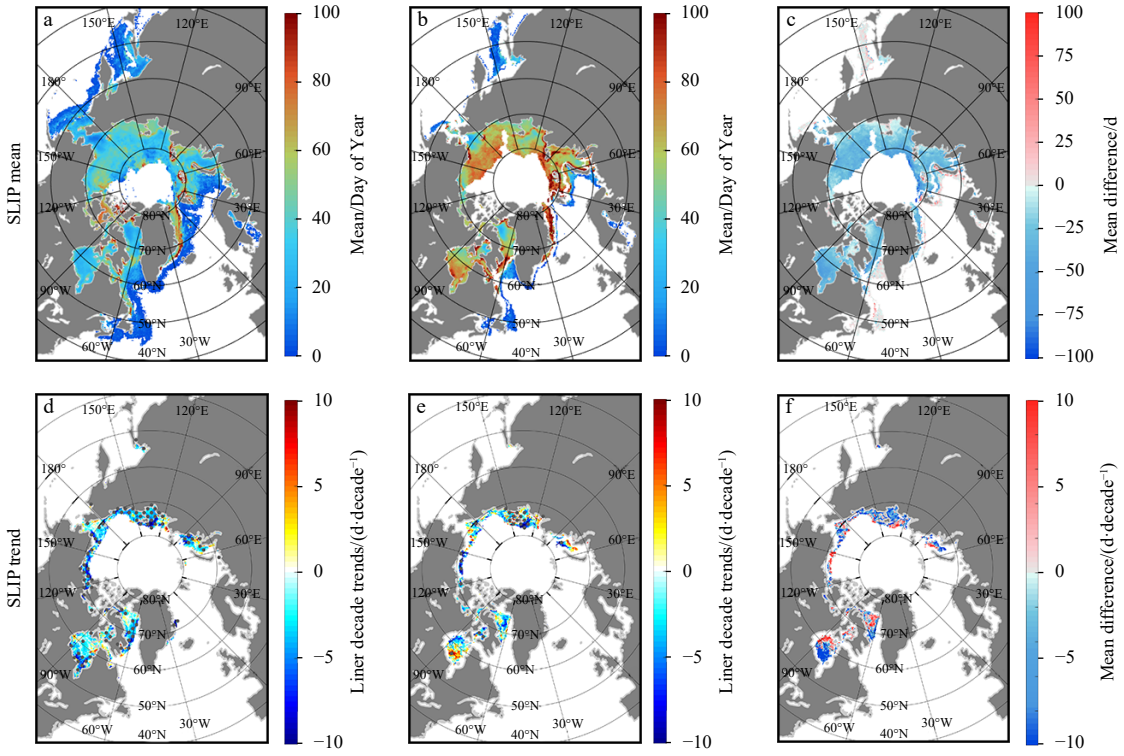

Fig. 7. Mean and linear decadal trends of seasonal loss of ice period (SLIP) for the period of 1982–2017 derived from Bootstrap Team sea ice concentration (BT SIC), i.e., bSLIP mean (a) and bSLIP trend (d), and NASA Team sea ice concentration (NT SIC), i.e., nSLIP mean (b) and nSLIP trend (e). The differences (BT result minus NT result) between the two estimations (c, f) are also shown. Trends are calculated only in locations where melt pond formation period (MPFP) or melt pond extension period (MPEP) occurs in more than 80% of the years over the entire record. Black points indicate that the pixels are significant at the 95% confidence level.

where bSLIP was approximately equal to or slightly greater than nSLIP (Figs 7a–c). Smaller DOR combined with greater DOO in the BT SIC contributed to a generally shorter bSLIP. The sectorial-mean of the length of bSLIP was less than 60 d, except for the Canadian Arctic Archipelago, which was predominated by multi-year ice (Hunke and Bitz, 2009). The length of nSLIP was over 60 d in the Arctic Ocean, Hudson Bay, and the Greenland Sea, where their SLIPs were about 30 d longer than bSLIP. The SLIP was shortest in the Sea of Okhotsk, Bering Sea, and Baffin Bay in BT and NT results; they varied between 15 d and 24 d in bSLIP and ranged from 12 d to 40 d in nSLIP.

The length of the SLIP denoted negative trends in all sub-regions in BT and NT results with an overall sectorial-mean of –2.61 d/decade in bSLIP and –1.06 d/decade in nSLIP, respectively (Figs 7d, e; Table 1); and the greatest decreasing trend was found in the Greenland Sea (–5.75 d/decade in bSLIP) in both results. Among the exceptions are the Sea of Okhotsk (1.07 d/decade) and Bering Sea (zero) in nSLIP, which resulted from little ice retreating on a yearly basis. The shorter SLIP over the Arctic was likely due to a decrease of more than 50% in multi-year ice since 2002, which resulted in a poleward retreat of ice edge as a norm, thereby indicating that full sea ice underwent a quicker transition to open water in melt season from year to year (Strong and Rigor, 2013; Kwok, 2018).

4.3 *Temporal evolution of the sea ice surface melt*

The average trends of four timings and three durations of the melt season for all sub-domains in the Arctic are summarized in Table 2, only locations where ice underwent MO, PO, and DOR in turn in both BT and NT results were counted. Large interannual variability in timings was evident. All timings determined by BT SIC showed an upward trend in all areal-mean statistics except for bDOR, whereas timings generated from NT SIC were trending later except nDOO and nDOR. All areal-mean PO exhibited a slight and non-significant upward trend of 0.2 d/decade and 0.3 d/decade in NT and BT results, respectively (Table 2). However, all durations presented a weak downward trend in BT and NT results over the whole Arctic (Table 2). Compared with durations obtained from NT SIC, larger and significant trends occurred in durations from BT SIC.

The mean annual evolution of the sea ice surface melt based on BT and NT results in the Arctic from 1982 to 2017 is shown in Fig. 8. Two MO were identical as they were generated from NSIDC MO directly, ranging from late-April to mid-May. The sea ice started ponding around late May and showed earlier bPO in comparison with nPO, whereas no significant difference was found between bPO and nPO with all areal-means of less than 4 d, leading to 4 d shorter bMPFP compared with nMPFP. The nDOO preceded or coincided with nPO from mid-May to early June, indicating that sea ice experienced MO, PO, and DOR in the Hudson Bay, the Baffin Bay, the Greenland Sea, Kara and Barents seas, and the periphery of the western Arctic Ocean in NASA Team results (Figs 4b and 5b; Table 2). The bDOO minus bPO varied between 15 d and 26 d from year to year, denoting that valid PO occurred along the periphery of the Arctic Ocean and the Kara Sea, the west corner of the Sea of Okhotsk, the southern Hudson Bay, and the Greenland Sea (Figs 4a and 5a). In general, it took about 28 d and 31 d for ice to form ponds since MO in BT SIC and NT SIC, respectively. Later, the melt ponds grew for 58 d and 50 d until ice retreated in two SIC products, respectively.

Table 2. Regional decadal trends (d/decade) in phenology factors are presented. Only locations that underwent MO, PO, and DOR in turn are included (i.e., Method II). Except for MO, the first and second rows for each factor represent the results derived from Bootstrap and NASA Team, respectively

Indicators	All	Sea of Okhotsk	Bering Sea	Hudson Bay	Baffin Bay	Greenland Sea	Kara & Barents seas	Arctic Ocean	Canadian Artic
MO (BT/NT)	0.6	3.0	5.4	2.8	–1.5	3.2	–1.5	–2.8*	0.1
PO (BT)	0.2	3.7	3.0	2.4	–1.3	4.6*	–1.2	–1.6**	–1.5*
PO (NT)	0.3	3.7	3.1	1.4	–1.2	4.0*	–0.5	–1.4*	–1.8**
DOO (BT)	1.1*	1.0	4.9	–0.3	–2.2	1.3	–3.9*	0.2	–1.0
DOO (NT)	–0.1	0.1	6.8	2.5	–3.6	3.7	–4.2*	–2.2*	–1.1
DOR (BT)	–1.2	–1.2	5.9*	–0.5	–4.2**	–4.0	–6.1**	–2.3*	–4.5**
DOR (NT)	–0.2	–0.1	2.2	–0.5	–3.7**	–2.4	–5.5**	–1.0	–1.5
MPFP (BT)	–0.5	0.6	–2.4	–0.3	0.2	1.2	0	1.1	–1.6
MPFP (NT)	–0.4	0.6	–2.3	–1.3	0.3	0.5	0.7	1.3	–1.9*
MPEP (BT)	–1.4*	–4.9	2.9	–2.9*	–3.0	–8.5**	–4.9**	–0.6	–3.0*
MPEP (NT)	–0.5	–3.7	–0.9	–2.0	–2.5	–6.4*	–5.1**	0.5	0.3
SLIP (BT)	–2.3**	–2.2	1.0	–0.2	–2.0	–5.3	–2.2*	–2.4**	–3.5**
SLIP (NT)	0	–0.1	–4.7	–3.0	–0.1	–6.1	–1.3	1.3	–0.5

Note: Significant levels of trends are noted as 95% (*) and 99% (**).

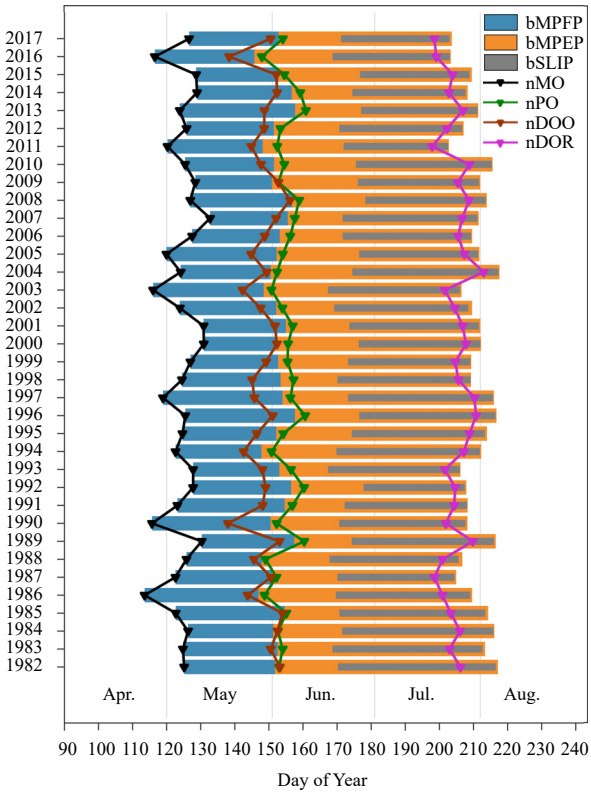

Fig. 8. Mean annual evolution of the sea ice surface melt in the Arctic from 1982 to 2017. Blue, orange, and gray shaded bars define the mean MPFP (bMPFP), MPEP (bMPEP), and SLIP (bSLIP) obtained from BT SIC, respectively. The beginning and ending points of these bars denote the annual mean MO (bMO), PO (bPO), DOO (bDOO), and DOR (bDOR) derived from BT SIC. The timings determined from NT SIC are presented in curves. The black, green, red, and violet curves noted with filled triangles show annual mean MO (nMO), PO (nPO), DOO (nDOD), and DOR (nDOR), respectively. The span of each two contiguous curves denotes nMPFP, nMPEP, and nSLIP.

4.4 *Outlook and discussion*

In comparison to previous studies, the spatial distribution of mean MO and area-averaged bSLIP in the pan-Arctic in our study are in good agreement with that got by Peng et al. (2018). The trends of MO in sub-regions excluding the Greenland Sea and mean bSLIP over the Arctic are in line with results reported by Bliss et al. (2019) and Singh et al. (2021), whereas nSLIP was ~15 d longer. However, a significant decreasing trend of –2.6 d/decade was observed in the Canadian Arctic Archipelago, which is different from that by Mahmud et al. (2016). A lower value in BT SIC and NT SIC compared with CDR concentration (Meier et al., 2014), resulting in more than 30 d earlier in DOO and DOR (Peng et al., 2018; Bliss et al., 2019). Nevertheless, the DOO, DOR, and SLIP extracted from BT and NT SIC products revealed significant downward trends over the Arctic, consistent with the results by Bliss et al. (2019) and almost identical to those reported by Peng et al. (2018). The exceptional regions were the marginal ice zone viz., Sea of Okhotsk and the Bering Sea, where had high uncertainties in SIC products (Comiso et al., 1997; Meier et al., 2014).

The correlation coefficient matrix demonstrates that MO predominates PO. A strong correlation not only occurred between MO and PO, but also was exhibited between MO and MPFP in both BT and NT results (Tables A3 and A4). Our results support the conclusion that the MO was the dominant forcing setting the PO (Skyllingstad and Polashenski, 2018) and predominated the progress of pond formation. A clear correlation was demonstrated between PO and DOO in BT and NT results but not found between PO and DOR, indicating that ponding water only made a difference during melt season when SIC was high.

Ponding ice transmitted from full ice cover to open water quickly. Because of different counting strategies, Tables 1 and 2 revealed different regional decadal trends and even exhibited opposite trends in most phenology factors. However, SLIP and newly proposed durations of MPFP and MPEP derived from BT results suggested a weak decreasing trend over the Arctic in both methods. Although NT results did not capture these changes, we can draw a firm conclusion that less time is needed for ponding ice to melt out over the last 36 years, considering that both the bias and the error standard deviation of the BT SIC are smaller or comparable with those derived from the NT SIC (Andersen et al., 2007).

The uncertainty of the PO detection algorithm has a substantial impact on determined PO, MPFP, and MPEP. We used a fixed threshold in albedo to detect PO over the Arctic without consid-

ering the differences between first-year ice and multi-year ice in the characteristics. An adaptive threshold that is based on ice identities may lead to more precise PO in the future. Moreover, sea ice advection affected detected PO as well. The retrieved PO in a specified region is not only related to the onset of snow and sea ice surface melt, but also may be attributed to sea ice floes with lower albedo drifted from near regions. Hence, more precise results associated with PO can be obtained after tracking sea ice drift. In addition, leads formation and sea ice deformation associated with sea ice drift also contributed to changes in ice surface albedo (Tucker III et al., 1999; Perovich et al., 2001; Perovich, 2018).

High-resolution albedo data are needed to determine PO better, because melt ponds have widths ranging from meters to hundreds of meters (Zege et al., 2015). With the limitation of microwave radiometer sensors to distinguish water in melt ponds from the water in leads, CDR SIC and BT SIC overestimate the true concentration, whereas NT SIC provides an underestimated measure (Kern et al., 2020). Nonetheless, the variability of factors associated with SIC is convictive because of the good agreement in trends among these products. A more precise SIC product, such as SIC from the European Organization for the Exploitation of Meteorological Satellites Ocean and Sea Ice Satellite Application Facility (Tonboe et al., 2016; Lavergne et al., 2019), could better elucidate ice dynamics.

5 Conclusions

Temporal means and trends of the Arctic summer sea ice phenology derived from BT SIC and NT SIC were presented. These phenology factors with newly proposed PO and corresponding periods were used to track the evolution of the Arctic melting sea ice from 1982 to 2017. For the entire Arctic, the average PO was nearly 4 d earlier in BT results compared with that of NT results; these dates ranged from late April in the peripheral seas to late June in the central Arctic Ocean. In general, DOO and DOR determined by BT SIC were later than those determined by NT SIC, with an average over 30 d difference appearing in the Hudson Bay and the Arctic Ocean for DOO. The DOR occurred from March to October in BT SIC, whereas it began in April and finished in September, which corresponded with the DOO in NT SIC. The length of regional MPFP obtained from BT results varied between 24 d in the Canadian Arctic Archipelago and 56 d in the Bering Sea, and all areal-mean MPFPs were slightly 3.7 d longer than those in the NT results. Conversely, MPEP in BT results ranged from 18.9 d in the Bering Sea to 87.5 d in the Greenland Sea, which was on average 4.8 d longer than that from NT results over the Arctic. As for SLIP, bSLIP was approximately 14 d shorter than nSLIP. The high correlation coefficient between MO and PO, MPFP illustrated that MO predominates the process of pond formation. A slight decreasing trend in bMPFP, bMPEP, and bSLIP denoted that ponding ice transmitted from full ice cover to open water quickly over the Arctic. Limitations concerning sea ice advection and fixed threshold set constraints on PO detection. Despite this, our findings suggest new possibilities to predict ice evolution in the Arctic.

Acknowledgements

The authors sincerely acknowledge the National Snow and Ice Data Center for providing the yearly surface melt onset dates, NASA Team SIC, and Bootstrap Algorithm SIC. The authors are deeply grateful for the sea ice albedo product provided by NOAA National Centers for Environmental Information.

References

Andersen S, Tonboe R, Kaleschke L, et al. 2007. Intercomparison of passive microwave sea ice concentration retrievals over the high-concentration Arctic sea ice. Journal of Geophysical Research: Oceans, 112(C8): C08004, doi: 10.1029/2006JC003543

Anderson M R. 1997. Determination of a melt-onset date for Arctic sea-ice regions using passive-microwave data. Annals of Glaciology, 25: 382–387, doi: 10.3189/S0260305500014324

Anderson M, Bliss A C, Drobot S. 2019. Snow melt onset over Arctic sea ice from SMMR and SSM/I-SSMIS brightness temperatures, version 4. Boulder, CO: NASA National Snow and Ice Data Center Distributed Active Archive Center, doi: 10.5067/A9YK15H5EBHK

Bi Haibo, Zhang Jinlun, Wang Yunhe, et al. 2018. Arctic sea ice volume changes in terms of age as revealed from satellite observations. IEEE Journal of Selected Topics in Applied Earth Observations and Remote Sensing, 11(7): 2223–2237, doi: 10.1109/JSTARS.2018.2823735

Bliss A C, Anderson M R. 2018. Arctic sea ice melt onset timing from passive microwave-based and surface air temperature-based methods. Journal of Geophysical Research: Atmospheres, 123(17): 9063–9080, doi: 10.1029/2018JD028676

Bliss A C, Miller J A, Meier W N. 2017. Comparison of passive microwave-derived early melt onset records on Arctic sea ice. Remote Sensing, 9(3): 199, doi: 10.3390/rs9030199

Bliss A C, Steele M, Peng Ge, et al. 2019. Regional variability of Arctic sea ice seasonal change climate indicators from a passive microwave climate data record. Environmental Research Letters, 14(4): 045003, doi: 10.1088/1748-9326/aafb84

Cavalieri D J, Gloersen P, Campbell W J. 1984. Determination of sea ice parameters with the Nimbus 7 SMMR. Journal of Geophysical Research: Atmospheres, 89(D4): 5355–5369, doi: 10.1029/JD089iD04p05355

Cavalieri D J, Parkinson C L. 2012. Arctic sea ice variability and trends, 1979-2010. The Cryosphere, 6(4): 881–889, doi: 10.5194/tc-6-881-2012

Comiso J C. 1995. SSM/I sea ice concentrations using the bootstrap algorithm. Greenbelt: NASA

Comiso J C. 2012. Large decadal decline of the Arctic multiyear ice cover. Journal of Climate, 25(4): 1176–1193, doi: 10.1175/JCLI-D-11-00113.1

Comiso J C, Cavalieri D J, Parkinson C L, et al. 1997. Passive microwave algorithms for sea ice concentration: a comparison of two techniques. Remote Sensing of Environment, 60(3): 357–384, doi: 10.1016/S0034-4257(96)00220-9

Comiso J C, Parkinson C L, Gersten R, et al. 2008. Accelerated decline in the Arctic sea ice cover. Geophysical Research Letters, 35(1): L01703, doi: 10.1029/2007GL031972

Curry J A, Schramm J L, Ebert E E. 1995. Sea ice-albedo climate feedback mechanism. Journal of Climate, 8(2): 240–247, doi: 10.1175/1520-0442(1995)008<0240:SIACFM>2.0.CO;2

Flocco D, Feltham D L, Bailey E, et al. 2015. The refreezing of melt ponds on Arctic sea ice. Journal of Geophysical Research: Oceans, 120(2): 647–659, doi: 10.1002/2014JC010140

Flocco D, Schroeder D, Feltham D L, et al. 2012. Impact of melt ponds on Arctic sea ice simulations from 1990 to 2007. Journal of Geophysical Research: Oceans, 117(C9): C09032

Fors A S, Divine D V, Doulgeris A P, et al. 2017. Signature of Arctic first-year ice melt pond fraction in X-band SAR imagery. The Cryosphere, 11(2): 755–771, doi: 10.5194/tc-11-755-2017

Frey K E, Moore G W K, Cooper L W, et al. 2015. Divergent patterns of recent sea ice cover across the Bering, Chukchi, and Beaufort seas of the Pacific Arctic Region. Progress in Oceanography, 136: 32–49, doi: 10.1016/j.pocean.2015.05.009

Grenfell T C, Perovich D K. 2004. Seasonal and spatial evolution of albedo in a snow-ice-land-ocean environment. Journal of Geophysical Research: Oceans, 109(C1): C01001, doi: 10.1029/2003jc001866

Holland M M, Bailey D A, Briegleb B P, et al. 2012. Improved sea ice shortwave radiation physics in CCSM4: the impact of melt ponds and aerosols on Arctic sea ice. Journal of Climate, 25(5):

1413–1430, doi: 10.1175/JCLI-D-11-00078.1
Holland M M, Bitz C M, Tremblay B. 2006. Future abrupt reductions in the summer Arctic sea ice. Geophysical Research Letters, 33(23): L23503, doi: 10.1029/2006GL028024
Huang Wenfeng, Lu Peng, Lei Ruibo, et al. 2016. Melt pond distribution and geometry in high Arctic sea ice derived from aerial investigations. Annals of Glaciology, 57(73): 105–118, doi: 10.1017/aog.2016.30
Hunke E C, Bitz C M. 2009. Age characteristics in a multidecadal Arctic sea ice simulation. Journal of Geophysical Research: Oceans, 114(C8): C08013, doi: 10.1029/2008JC005186
Hunke E C, Hebert D A, Lecomte O. 2013. Level-ice melt ponds in the Los Alamos sea ice model, CICE. Ocean Modelling, 71: 26–42, doi: 10.1016/j.ocemod.2012.11.008
Istomina L, Heygster G, Huntemann M, et al. 2015a. Melt pond fraction and spectral sea ice albedo retrieval from MERIS data-Part 2: case studies and trends of sea ice albedo and melt ponds in the Arctic for years 2002–2011. The Cryosphere, 9(4): 1567–1578, doi: 10.5194/tc-9-1567-2015
Istomina L, Heygster G, Huntemann M, et al. 2015b. Melt pond fraction and spectral sea ice albedo retrieval from MERIS data-Part 1: validation against *in situ*, aerial, and ship cruise data. The Cryosphere, 9(4): 1551–1566, doi: 10.5194/tc-9-1551-2015
Kern S, Lavergne T, Notz D, et al. 2020. Satellite passive microwave sea-ice concentration data set inter-comparison for Arctic summer conditions. The Cryosphere, 14(7): 2469–2493, doi: 10.5194/tc-14-2469-2020
Key J, Wang Xuanji, Liu Yinghui, et al. 2016. The AVHRR polar pathfinder climate data records. Remote Sensing, 8(3): 167, doi: 10.3390/rs8030167
Kim J M, Sohn B J, Lee S M, et al. 2020. Differences between ICESat and CryoSat-2 sea ice thicknesses over the Arctic: consequences for analyzing the ice volume trend. Journal of Geophysical Research: Atmospheres, 125(22): e2020JD033103, doi: 10.1029/2020JD033103
Kouki K, Anttila K, Manninen T, et al. 2019. Intercomparison of snow melt onset date estimates from optical and microwave satellite instruments over the northern hemisphere for the period 1982–2015. Journal of Geophysical Research: Atmospheres, 124(21): 11205–11219, doi: 10.1029/2018JD030197
Kumar A, Yadav J, Mohan R. 2021. Spatio-temporal change and variability of Barents-Kara sea ice, in the Arctic: ocean and atmospheric implications. Science of the Total Environment, 753: 142046, doi: 10.1016/j.scitotenv.2020.142046
Kwok R. 2018. Arctic sea ice thickness, volume, and multiyear ice coverage: losses and coupled variability (1958–2018). Environmental Research Letters, 13(10): 105005, doi: 10.1088/1748-9326/aae3ec
Kwok R, Cunningham G F. 2015. Variability of Arctic sea ice thickness and volume from CryoSat-2. Philosophical Transactions of the Royal Society A: Mathematical, Physical and Engineering Sciences, 373(2045): 20140157, doi: 10.1098/rsta.2014.0157
Kwok R, Cunningham G F, Wensnahan M, et al. 2009. Thinning and volume loss of the Arctic Ocean sea ice cover: 2003–2008. Journal of Geophysical Research: Oceans, 114(C7): C07005, doi: 10.1029/2009JC005312
Landy J C, Ehn J K, Barber D G. 2015. Albedo feedback enhanced by smoother Arctic sea ice. Geophysical Research Letters, 42(24): 10714–10720, doi: 10.1002/2015GL066712
Lavergne T, Sørensen A M, Kern S, et al. 2019. Version 2 of the EUMETSAT OSI SAF and ESA CCI sea-ice concentration climate data records. The Cryosphere, 13(1): 49–78, doi: 10.5194/tc-13-49-2019
Lei Ruibo, Li Zhijun, Li Na, et al. 2012. Crucial physical characteristics of sea ice in the Arctic section of 143°–180°W during August and early September 2008. Acta Oceanologica Sinica, 31(4): 65–75, doi: 10.1007/s13131-012-0221-0
Lei Ruibo, Tian-Kunze X, Leppäranta M, et al. 2016. Changes in summer sea ice, albedo, and portioning of surface solar radiation in the Pacific sector of Arctic Ocean during 1982–2009. Journal of Geophysical Research: Oceans, 121(8): 5470–5486, doi: 10.1002/2016JC011831
Li Lanyu, Ke Changqing, Xie Hongjie, et al. 2017b. Aerial observations of sea ice and melt ponds near the North Pole during CHINARE2010. Acta Oceanologica Sinica, 36(1): 64–72, doi: 10.1007/s13131-017-0994-2
Li Haiyan, Perrie W, Li Qun, et al. 2017a. Estimation of melt pond fractions on first year sea ice using compact polarization SAR. Journal of Geophysical Research: Oceans, 122(10): 8145–8166, doi: 10.1002/2017JC013248
Li Qing, Zhou Chunxia, Zheng Lei, et al. 2020. Monitoring evolution of melt ponds on first-year and multiyear sea ice in the Canadian Arctic Archipelago with optical satellite data. Annals of Glaciology, 61(82): 154–163, doi: 10.1017/aog.2020.24
Light B, Perovich D K, Webster M A, et al. 2015. Optical properties of melting first-year Arctic sea ice. Journal of Geophysical Research: Oceans, 120(11): 7657–7675, doi: 10.1002/2015JC011163
Lindsay R, Schweiger A. 2015. Arctic sea ice thickness loss determined using subsurface, aircraft, and satellite observations. The Cryosphere, 9(1): 269–283, doi: 10.5194/tc-9-269-2015
Lu Peng, Cao Xiaowei, Wang Qingkai, et al. 2018a. Impact of a surface ice lid on the optical properties of melt ponds. Journal of Geophysical Research: Oceans, 123(11): 8313–8328, doi: 10.1029/2018JC014161
Lu Peng, Leppäranta M, Cheng Bin, et al. 2018b. The color of melt ponds on Arctic sea ice. The Cryosphere, 12(4): 1331–13455, doi: 10.5194/tc-12-1331-2018
Ma Y P, Sudakov I, Strong C, et al. 2019. Ising model for melt ponds on Arctic sea ice. New Journal of Physics, 21(6): 063029, doi: 10.1088/1367-2630/ab26db
Mahmud M S, Howell S E L, Geldsetzer T, et al. 2016. Detection of melt onset over the northern Canadian Arctic Archipelago sea ice from RADARSAT, 1997–2014. Remote Sensing of Environment, 178: 59–69, doi: 10.1016/j.rse.2016.03.003
Markus T, Cavalieri D J, Tschudi M A, et al. 2003. Comparison of aerial video and Landsat 7 data over ponded sea ice. Remote Sensing of Environment, 86(4): 458–469, doi: 10.1016/S0034-4257(03)00124-X
Markus T, Stroeve J C, Miller J. 2009. Recent changes in Arctic sea ice melt onset, freezeup, and melt season length. Journal of Geophysical Research: Oceans, 114(C12): C12024, doi: 10.1029/2009JC005436
Maslanik J A, Fowler C, Stroeve J, et al. 2007. A younger, thinner Arctic ice cover: increased potential for rapid, extensive sea-ice loss. Geophysical Research Letters, 34(24): L24501, doi: 10.1029/2007GL032043
Matthews J L, Peng Ge, Meier W N, et al. 2020. Sensitivity of Arctic sea ice extent to sea ice concentration threshold choice and its implication to ice coverage decadal trends and statistical projections. Remote Sensing, 12(5): 807, doi: 10.3390/rs12050807
Meier W N, Peng Ge, Scott D J, et al. 2014. Verification of a new NOAA/NSIDC passive microwave sea-ice concentration climate record. Polar Research, 33(1): 21004, doi: 10.3402/polar.v33.21004
Nicolaus M, Katlein C. 2013. Mapping radiation transfer through sea ice using a remotely operated vehicle (ROV). The Cryosphere, 7(3): 763–777, doi: 10.5194/tc-7-763-2013
Onarheim I H, Eldevik T, Smedsrud L H, et al. 2018. Seasonal and regional manifestation of Arctic sea ice loss. Journal of Climate, 31(12): 4917–4932, doi: 10.1175/JCLI-D-17-0427.1
Pegau W S, Paulson C A. 2001. The albedo of Arctic leads in summer. Annals of Glaciology, 33: 221–224, doi: 10.3189/172756401781818833
Peng Ge, Meier W N. 2018. Temporal and regional variability of Arctic sea-ice coverage from satellite data. Annals of Glaciology, 59(76pt2): 191–200, doi: 10.1017/aog.2017.32
Peng Ge, Steele M, Bliss A C, et al. 2018. Temporal means and variability of Arctic sea ice melt and freeze season climate indicators using a satellite climate data record. Remote Sensing, 10(9): 1328, doi: 10.3390/rs10091328
Perovich D K. 2018. Sunlight, clouds, sea ice, albedo, and the radiative budget: the umbrella versus the blanket. The Cryosphere,

12(6): 2159–2165, doi: 10.5194/tc-12-2159-2018
Perovich D K, Nghiem S V, Markus T, et al. 2007. Seasonal evolution and interannual variability of the local solar energy absorbed by the Arctic sea ice-ocean system. Journal of Geophysical Research: Oceans, 112(C3): C03005, doi: 10.1029/2006JC003558
Perovich D K, Polashenski C. 2012. Albedo evolution of seasonal Arctic sea ice. Geophysical Research Letters, 39(8): L08501
Perovich D K, Richter-Menge J A, Tucker III W B. 2001. Seasonal changes in Arctic sea-ice morphology. Annals of Glaciology, 33: 171–176, doi: 10.3189/172756401781818716
Perovich D K, Tucker III W B, Ligett K A. 2002. Aerial observations of the evolution of ice surface conditions during summer. Journal of Geophysical Research: Oceans, 107(C10): 8048, doi: 10.1029/2000JC000449
Polashenski C, Perovich D, Courville Z. 2012. The mechanisms of sea ice melt pond formation and evolution. Journal of Geophysical Research: Oceans, 117(C1): C01001
Rösel A, Kaleschke L. 2012. Exceptional melt pond occurrence in the years 2007 and 2011 on the Arctic sea ice revealed from MODIS satellite data. Journal of Geophysical Research: Oceans, 117(C5): C05018
Rösel A, Kaleschke L, Birnbaum G. 2012. Melt ponds on Arctic sea ice determined from MODIS satellite data using an artificial neural network. The Cryosphere, 6(2): 431–446, doi: 10.5194/tc-6-431-2012
Scharien R K, Landy J, Barber D G. 2014. First-year sea ice melt pond fraction estimation from dual-polarisation C-band SAR-Part 1: *in situ* observations. The Cryosphere, 8(6): 2147–2162, doi: 10.5194/tc-8-2147-2014
Scott F, Feltham D L. 2010. A model of the three-dimensional evolution of Arctic melt ponds on first-year and multiyear sea ice. Journal of Geophysical Research: Oceans, 115(C12): C12064, doi: 10.1029/2010JC006156
Shu Qi, Wang Qiang, Song Zhenya, et al. 2021. The poleward enhanced Arctic Ocean cooling machine in a warming climate. Nature Communications, 12(1): 2966, doi: 10.1038/s41467-021-23321-7
Singh R K, Singh T V, Singh U S. 2021. Long-term observation of the Arctic sea ice melt onset from microwave radiometry. Journal of the Indian Society of Remote Sensing, 49(2): 357–364, doi: 10.1007/s12524-020-01220-6
Skagseth Ø, Eldevik T, Årthun M, et al. 2020. Reduced efficiency of the Barents Sea cooling machine. Nature Climate Change, 10(7): 661–666, doi: 10.1038/s41558-020-0772-6
Skyllingstad E D, Polashenski C. 2018. Estimated heat budget during summer melt of Arctic first-year sea ice. Geophysical Research Letters, 45(21): 11789–11797, doi: 10.1029/2018GL080349
Stammerjohn S, Massom R, Rind D, et al. 2012. Regions of rapid sea ice change: an inter-hemispheric seasonal comparison. Geophysical Research Letters, 39(6): L06501, doi: 10.1029/2012GL050874
Steele M, Dickinson S. 2016. The phenology of Arctic Ocean surface warming. Journal of Geophysical Research: Oceans, 121(9): 6847–6861, doi: 10.1002/2016JC012089
Steele M, Dickinson S, Zhang Jinlun, et al. 2015. Seasonal ice loss in the Beaufort Sea: toward synchrony and prediction. Journal of Geophysical Research: Oceans, 120(2): 1118–1132, doi: 10.1002/2014JC010247
Steele M, Ermold W, Zhang Jinlun. 2008. Arctic Ocean surface warming trends over the past 100 years. Geophysical Research Letters, 35(2): L02614, doi: 10.1029/2007GL031651
Stroeve J C, Serreze M C, Holland M M, et al. 2012. The Arctic's rapidly shrinking sea ice cover: a research synthesis. Climatic Change, 110(3–4): 1005–1027, doi: 10.1007/s10584-011-0101-1
Strong C, Rigor I G. 2013. Arctic marginal ice zone trending wider in summer and narrower in winter. Geophysical Research Letters, 40(18): 4864–4868, doi: 10.1002/grl.50928
Tonboe R T, Eastwood S, Lavergne T, et al. 2016. The EUMETSAT sea ice concentration climate data record. The Cryosphere, 10(5): 2275–2290, doi: 10.5194/tc-10-2275-2016
Tschudi M A, Maslanik J A, Perovich D K. 2008. Derivation of melt pond coverage on Arctic sea ice using MODIS observations. Remote Sensing of Environment, 112(5): 2605–2614, doi: 10.1016/j.rse.2007.12.009
Tucker III W B, Gow A J, Meese D A, et al. 1999. Physical characteristics of summer sea ice across the Arctic Ocean. Journal of Geophysical Research: Oceans, 104(C1): 1489–1504, doi: 10.1029/98JC02607
Untersteiner N. 1961. On the mass and heat budget of Arctic sea ice. Archiv für Meteorologie, Geophysik und Bioklimatologie, Serie A, 12(2): 151–182, doi: 10.1007/BF02247491
Wang Zongliang, Li Zhen, Zeng Jiangyuan, et al. 2020. Spatial and temporal variations of Arctic sea ice from 2002 to 2017. Earth and Space Science, 7(9): e2020EA001278, doi: 10.1029/2020EA001278
Webster M A, Rigor I G, Perovich D K, et al. 2015. Seasonal evolution of melt ponds on Arctic sea ice. Journal of Geophysical Research: Oceans, 120(9): 5968–5982, doi: 10.1002/2015JC011030
Wu Zhankai, Wang Xiongdong. 2019. Variability of Arctic sea ice (1979–2016). Water, 11(1): 23, doi: 10.3390/w11010023
Zege E, Malinka A, Katsev I, et al. 2015. Algorithm to retrieve the melt pond fraction and the spectral albedo of Arctic summer ice from satellite optical data. Remote Sensing of Environment, 163: 153–164, doi: 10.1016/j.rse.2015.03.012
Zheng Lei, Cheng Xiao, Chen Zhuoqi, et al. 2021. Delay in Arctic sea ice freeze-up linked to early summer sea ice loss: evidence from satellite observations. Remote Sensing, 13(11): 2162, doi: 10.3390/rs13112162
Zheng Jiacheng, Geldsetzer T, Yackel J. 2017. Snow thickness estimation on first-year sea ice using microwave and optical remote sensing with melt modelling. Remote Sensing of Environment, 199: 321–332, doi: 10.1016/j.rse.2017.06.038

Appendix:

Table A1. Acronyms, definitions, and descriptions of dates and periods, adapted from Peng et al. (2018)

Acronym	Definition and description
MO	date of snow and ice surface melt onset
PO	date of melt pond formation onset
DOO	date of opening, last day sea ice concentration drops below 80% before the first summer minimum
DOR	date of retreat, last day sea ice concentration drops below 15% before the first summer minimum
MPFP	melt pond formation period, defined as MO–PO
MPEP	melt pond extension period, defined as PO–DOR
SLIP	seasonal loss of ice period, defined as DOO–DOR

Table A2. Regional mean (d) of indicators

Indicators	All	Sea of Okhotsk	Bering Sea	Hudson Bay	Baffin Bay	Greenland Sea	Kara & Barents seas	Arctic Ocean	Canadian Arctic
MO	100.9	70.0	69.7	107.0	90.7	83.9	98.1	150.1	147.3
PO (BT)	140.7	124.1	127.6	141.3	136.7	125.4	127.6	166.8	167.7
PO (NT)	144.6	128.8	132.7	143.8	140.3	128.9	132.2	169.9	171.8
DOO (BT)	136.0	81.8	103.1	153.5	130.8	147.8	151.0	192.7	175.7
DOO (NT)	119.5	81.2	88.9	122.0	113.1	121.1	124.4	161.0	160.0
DOR (BT)	158.2	105.8	123.8	188.9	151.5	180.0	181.0	220.5	216.8
DOR (NT)	156.0	103.0	120.3	183.7	148.9	172.9	174.9	217.7	206.0
MPFP (BT)	40.2	44.4	56.0	37.4	43.5	46.5	38.0	25.3	24.0
MPFP (NT)	43.9	48.5	61.4	39.4	45.9	49.4	41.1	27.5	27.3
MPEP (BT)	47.3	20.9	18.9	52.0	42.8	87.5	64.0	62.4	58.7
MPEP (NT)	42.4	20.5	15.4	45.4	36.9	78.5	56.6	57.6	47.5
SLIP (BT)	26.9	12.1	18.2	36.6	25.7	46.2	38.9	38.1	51.0
SLIP (NT)	41.4	11.8	30.6	65.0	40.7	65.0	57.5	64.5	55.0

Note: All locations with a valid parameter were included. Except for MO, the first and second lines for each factor represent the results derived from Bootstrap and NASA Team, respectively (i.e., Method I).

Table A3. The correlation coefficients among all parameters derived from Bootstrap results

	bMO	bPO	bDOO	bDOR	bMPFP	bMPEP	bSLIP
bMO	1.00	**0.58**	0.39	0.24	**−0.73**	−0.20	−0.06
bPO		1.00	**0.60**	0.39	0.12	−0.37	−0.07
bDOO			1.00	0.43	0.00	−0.02	−0.35
bDOR				1.00	0.03	**0.72**	**0.70**
bMPFP					1.00	−0.07	0.02
bMPEP						1.00	**0.76**
bSLIP							1.00

Note: The correlation coefficients with absolute value greater than 0.5 are bolded.

Table A4. The correlation coefficients among all parameters derived from NASA-Team results

	nMO	nPO	nDOO	nDOR	nMPFP	nMPEP	nSLIP
nMO	1.00	**0.58**	**0.77**	0.33	**−0.69**	−0.19	−0.44
nPO		1.00	**0.55**	0.48	0.19	−0.44	−0.12
nDOO			1.00	0.33	−0.43	−0.17	**−0.65**
nDOR				1.00	0.01	**0.58**	**0.50**
nMPFP					1.00	−0.16	0.40
nMPEP						1.00	**0.62**
nSLIP							1.00

Note: The correlation coefficients with absolute value greater than 0.5 are bolded.